Determination of all scattering phases and amplitudes in the photodissociation of a diatomic molecule

Andrew Orr-Ewing, Oleg Vasyutinskii, Andrey Smolin

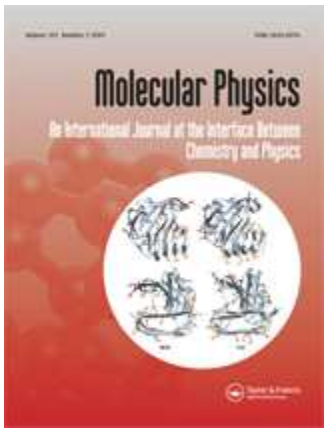

Determination of all scattering phases and amplitudes in the photodissociation of a diatomic molecule

Journal:	*Molecular Physics*
Manuscript ID:	TMPH-2006-0015
Manuscript Type:	Full Paper
Date Submitted by the Author:	04-Sep-2006
Complete List of Authors:	Orr-Ewing, Andrew; University of Bristol, School of Chemistry Vasyutinskii, Oleg; Ioffe Physico-Technical Institute Smolin, Andrey; Ioffe Physico-Technical Institute
Keywords:	photodissociation, non-adiabaticity, amplitude, phase, dynamics
Note: The following files were submitted by the author for peer review, but cannot be converted to PDF. You must view these files (e.g. movies) online.	
BrCl_phases_6.tex	

Determination of all scattering phases and amplitudes in the photodissociation of a diatomic molecule.

Andrey G. Smolin and Oleg S. Vasyutinskii*

Ioffe Physico-Technical Institute,

Russian Academy of Sciences,

194021 St.-Petersburg, Russia

Andrew J. Orr-Ewing†

School of Chemistry, University of Bristol, Bristol BS8 1TS, United Kingdom

(Dated: September 4, 2006)

Abstract

Analysis of the rank $K = 0-3$ anisotropy (orientation and alignment) parameters describing the angular momentum polarization of the Cl($^2P^0_{3/2}$) atoms formed from the 467-nm photodissociation of BrCl enables the relative phases and the amplitudes of the nuclear wavefunctions to be obtained for all of the five adiabatic potential energy curves with $\Omega = 0^+$ and 1 correlating to the lowest dissociation limit. A so-called "complete" experiment is thus demonstrated for photodissociation of this diatomic molecule in which all the components of the photofragmentation **T**-matrix are derived. Quantification of the amplitudes of dissociative flux on the $X^1\Sigma^+_{0+}$, $A^3\Pi_1$, $B^3\Pi_{0+}$, $C^1\Pi_1$ and D(1) states demonstrates the importance of non-adiabaticity in the dissociation dynamics. The relative phases contain contributions arising from nuclear motion on potential energy curves of different shapes in the short-range region, and from dynamical phase shifts associated with non-adiabatic transitions.

PACS: 33.80.Gj

*Author to whom correspondence should be addressed. E-mail:osv@pms.ioffe.ru

†Author to whom correspondence should be addressed. E-mail:A.Orr-Ewing@bristol.ac.uk

I. INTRODUCTION

The preferential polarization of the electronic angular momentum of atomic fragments following photodissociation of diatomic molecules with polarized ultraviolet or visible light contains valuable and very detailed information on the dissociation mechanism [1–3]. In general, multiple electronic states, each described by its own adiabatic potential energy curve, will correlate to two open-shell atomic products, and the route by which the system evolves from a molecular structure to two separated atoms may involve non-adiabatic transitions between these potential curves. A so-called "complete" photodissociation experiment [4] seeks to measure all the non-adiabatic transition probabilities (or, equivalently, the asymptotic amplitude on each potential energy curve correlating to the separated atom limit), and the phases of the nuclear wavefunctions on each adiabatic electronic potential - thus deriving the components of **T**-matrix elements used to treat the theory of photodissociation [5]. The polarization of the electronic angular momentum of the atoms is described most conveniently by the values of a set of orientation (odd rank) and alignment (even rank) parameters related to the state multipole moments of the electronic angular momentum density matrix. Measurement of these parameters provides a probe of the asymptotic amplitudes and phases of the dissociating nuclear wavefunctions, and thus direct information on **T**-matrix elements.

Several experimental studies have reported measurements of such orientation and alignment parameters (generically referred to hereafter as anisotropy parameters) for photodissociation of a variety of diatomic systems (see, for example, [6–16]), and results have been used to infer certain non-adiabatic crossing probabilities and phase shifts [10], as well as the shapes of molecular potential energy curves [17]. Theoretical analysis by Balint-Kurti and coworkers [2, 3] pointed the way to the determination of all amplitudes and phases of **T**-matrix elements, and illustrated the connection to anisotropy parameters by using wavepacket propagation to compute the photodissociation dynamics of HF and HCl. HF photodissociation is difficult to study experimentally, but detailed intercomparison between experiment and theory has been realized for HCl [3, 12], enabling the non-adiabatic dynamics to be understood quantitatively. Molecules such as these hydrogen halides are not, however, fully representative examples because their dissociation dynamics are dominated by electronic states with $|\Omega| = 1$ only (where Ω is the projection of the total angular momentum on the internuclear axis). Moreover, the fact that accurate theoretical studies of

the photodissociation dynamics are now tractable for HF and HCl meant that experimental data were not inverted to obtain phase and amplitude information; instead, theoretical predictions of the values of various anisotropy parameters, derived from calculated amplitudes and phases, were compared to experimental data.

Here, we demonstrate for the first time such an inversion of angular momentum polarization data for a molecule in which multiple, interacting electronic states of different symmetries ($|\Omega| = 0$ and 1) correlate to a single dissociation asymptote, and for which high-level electronic structure theory calculations cannot yet generate potential energy curves of sufficient accuracy for scattering calculations to provide a quantitative interpretation of experimental data. We chose to study the heteronuclear diatomic molecule BrCl, for which there are no simplifications imposed by inversion symmetry, such as forbidden interactions between states of u and g symmetry that occur, for example, in homonuclear molecules such as Cl_2. We demonstrate that, by measurement of a large number of the possible anisotropy parameters, a so-called "complete" photodissociation experiment can be realized, in which the amplitudes and phases of all relevant **T**-matrix elements are derived by inversion of experimental data. Realization of a "complete" experiment in the field of molecular dynamics is of great importance, as it provides a full set of information relating to the details of a photochemical process (at a particular excitation wavelength), thus stimulating progress in the development of both experimental techniques and new theoretical models.

Demonstration of this idea for a relatively simple system was recently reported for RbI photodissociation at 266 nm with circularly polarized light. Korovin et al. [15, 18] determined a single phase difference and the branching ratio of two amplitudes which completely describe the photodissociation dynamics through two molecular states of different symmetry.

The photodissociation dynamics of BrCl at a variety of visible and near-UV wavelengths have been the subject of extensive study in the Bristol laboratory using a high resolution photofragment velocity map imaging spectrometer [11, 16, 19, 20]. Wavepacket calculations of the dissociation dynamics following photoexcitation to the $A^3\Pi_1$, $B^3\Pi_{0+}$ and $C^1\Pi_1$ states, with allowance for non-adiabatic dynamics at the avoided crossing between the $B^3\Pi_{0+}$ state and a further $\Omega = 0^+$ state, were used to optimize the shapes of the potential energy curves, as shown in figure I [20], and successfully reproduced all wavelength-dependent measurements of branching ratios and photofragment translational anisotropies. The broad absorption spectrum of BrCl in the visible region of the spectrum was deconvoluted into

overlapping regions of excitation to these 3 dissociating states. Figure I also includes the ground $X^1\Sigma^+_{0+}$ state potential, and a schematic curve for what we refer to hereafter as the D(1) state, which is the third state with $\Omega = 1$ that correlates to ground state Br and Cl atoms. In the figure, the B state is illustrated by an adiabatic potential energy curve, with a maximum at 3.26 Angstroms caused by an avoided crossing with another $\Omega = 0^+$ state.

The experimental measurements culminated in successful evaluation of 12 of the 13 electronic angular momentum anisotropy parameters for the $Cl(^2P^0_{3/2})$ photofragment. Values for the rank $K = 0$ anisotropy parameter (β), four of the five rank $K = 2$ alignment parameters (α_2, s_2, γ_2, and η_2, but not γ'_2) and all the rank $K = 1$ and 3 orientation parameters (α_K, γ_K, γ'_K and η_K) were reported previously for 467-nm photodissociation of BrCl [11, 16]. These parameters describe the contributions to the angular momentum polarization from coherent and incoherent mechanisms involving parallel ($\Delta\Omega = 0$) and perpendicular ($\Delta\Omega = \pm 1$) photoexcitations to dissociative states. Here, we demonstrate how the anisotropy parameters are intimately connected to the **T**-matrix amplitudes and phases via expressions that are generally applicable to diatomic interhalogen molecules, and we describe the inversion of the experimentally measured anisotropy parameters. Although high quality diabatic potentials have been derived from experimental data [20], the couplings between the potentials are not known and thus wavepacket propagation methods cannot yet be used to compute either the anisotropy parameters or full **T**-matrix elements incorporating non-adiabatic dissociation dynamics for direct comparison with experimental results.

II. ANALYSIS AND RESULTS

In the axial recoil approximation for dissociation of a diatomic molecule AB, the fragment A state multipoles can be written as [1, 2]:

$$\rho_{KQ}(\theta,\phi) = \frac{3}{4\pi}\left(\frac{2K+1}{2j_A+1}\right)^{1/2} \sum_{k_d,q_d,Q'} \sum_{q,q'} (-1)^{K+q'} E_{k_d q_d}(\mathbf{e}) \frac{f_K(q,q')}{f_0(0,0)+2f_0(1,1)} \times (2k_d+1)^{1/2} \begin{pmatrix} 1 & 1 & k_d \\ q' & -q & -Q' \end{pmatrix} D^{K^*}_{QQ'}(\phi,\theta,0) D^{k_d}_{q_d Q'}(\phi,\theta,0), \quad (1)$$

where $D^K_{QQ'}(\phi,\theta,0)$ are Wigner rotation matrix elements [21], $Q' = q' - q$ is a component of the rank K state multipole in the molecular frame, and $E_{k_d q_d}(\mathbf{e})$ are elements of the

dissociation light polarization matrix [22, 23]. The dynamical functions, denoted by $f_K(q,q')$, contain all information about the photodissociation dynamics in the molecular frame. They can be expressed as [2]:

$$f_K(q,q') = \sum_{n,\Omega,\Omega_A,n',\Omega',\Omega'_A} (-1)^{K+j_A+\Omega'_A} \begin{pmatrix} j_A & j_A & K \\ -\Omega_A & \Omega'_A & q-q' \end{pmatrix} \mathcal{T}^{n\Omega}_{j_A\Omega_A j_B\Omega_B} (\mathcal{T}^{n'\Omega'}_{j_A\Omega'_A j_B\Omega_B})^* \times \langle \Psi^-_{n,\Omega}(R,\mathbf{r},E)|\hat{\mathbf{d}}_q|\Psi_{\Omega_i}\rangle^* \langle \Psi^-_{n',\Omega'}(R,\mathbf{r},E)|\hat{\mathbf{d}}_{q'}|\Psi_{\Omega_i}\rangle, \quad (2)$$

where $\langle \Psi^-_{n,\Omega}(R,\mathbf{r},E)|\hat{\mathbf{d}}_q|\Psi_{\Omega_i}\rangle$ are the photofragmentation **T**-matrix elements, connecting the ground and excited states with respective body fixed projections of the total angular momentum on the molecular axis of Ω_i and Ω (such that $\Omega = \Omega_i + q$).

In eq. (2), $\hat{\mathbf{d}}_q$ is a spherical component of the molecular electric dipole moment with respect to the recoil axis, q takes values of 0 and ± 1 respectively for parallel and perpendicular transitions, $\Psi^-_{n,\Omega}(R,\mathbf{r},E)$ is a scattering wavefunction for the state labelled by n and Ω, and $\mathcal{T}^{n\Omega}_{j_A\Omega_A j_B\Omega_B}$ is an expansion coefficient of the adiabatic electronic molecular wavefunctions at large separations in terms of the wavefunctions of the separate atoms basis set, $|j_A m_A, j_B, m_B\rangle$, with m_A the projection quantum number of the atomic angular momentum j_A on the recoil axis.

The anisotropy parameters for photofragment A that are measured in velocity map imaging experiments can be expressed as straightforward combinations of the dynamical functions, and thus relate directly to the **T**-matrix elements. The relevant relationships [2, 4, 8, 24] are reproduced below in the description of the data analysis.

The exact forms of the equations linking the dynamical functions and the **T**-matrix elements obtained by evaluation of eq. (2) depend upon the long range correlations of the adiabatic molecular potential energy curves to wavefunctions describing the separated fragments in an atomic basis set. If, as suggested by Balint-Kurti et al. [2], the **T**-matrix elements are written in terms of a modulus and a phase angle:

$$\langle \Psi^-_{n,\Omega}|\hat{\mathbf{d}}_q|\Psi_0\rangle = r_n e^{i\phi_n} \quad (3)$$

the dynamical functions can be presented in terms of the **T**-matrix amplitudes and phases.

For most of the studies undertaken to date [6, 7, 9, 10, 12, 14, 15], the number of interacting molecular quantum states was limited to 2-3. In these cases, the relationship between the dynamical functions and the **T**-matrix amplitudes and phases is straightforward and the

corresponding amplitudes and phases can be relatively easily determined from experimental data; see, for example, the review paper [25]. The more general case of multiple interacting electronic states of different symmetries which correlate to a single dissociation asymptote is the main subject of this paper.

For BrCl photodissociation, the quadrupole-quadrupole interaction between the atomic fragments is the major contribution to the long range potential energy, and the relationships between dynamical functions and phases and amplitudes can be expressed in the compact forms shown in Table I. These expressions are valid for other diatomic interhalogen molecules as well as for any other molecules where the same state symmetries arise from the Wigner-Witmer rules, the quadrupole-quadrupole interaction plays the major role in the long range and the signs of the atomic quadrupole moments are the same. These expressions are general in that they do not contain any assumptions about which of the excited states A, B, C, and D are optically populated from the ground state X. As usual, the square of each amplitude r_n in eq. (3) is proportional to the residual population of the corresponding molecular state arising from the optical excitation and the subsequent non-adiabatic interactions. For fast dissociation, such as is studied in this paper, only non-adiabatic interactions between states of the same symmetry ($\Omega = \Omega'$) are important, and the Coriolis type interactions between states of different symmetry ($\Omega = \Omega' \pm 1$) can usually be neglected.

It is immediately apparent from the expressions in Table I that the dynamical functions for BrCl photodissociation depend upon a large number of amplitudes and phases, describing the dissociation dynamics on three coupled potentials with $|\Omega| = 1$ and two potentials with $\Omega = 0^+$. The phase shifts between dissociative wavefunctions on potentials with different values of Ω also cannot be ignored. In the limit of adiabatic dissociation on the potentials accessed by the photoexcitation step, the expressions for the dynamical functions simplify greatly, but in the general case where non-adiabatic dynamics must be considered, inversion of experimental data to obtain all the phase and amplitude information is a challenging task.

The strategy employed in the current study to obtain values for all the amplitudes and phases of the **T**-matrix elements is to derive values for as many of the dynamical functions as is experimentally feasible. In practice, this means measuring as complete as possible a set of anisotropy parameters for the photofragment Cl($^2P^0_{3/2}$) atoms because these parameters are constructed from simple combinations of the dynamical functions. Table II lists the values of the anisotropy parameters obtained from experimental studies of Cl($^2P_{3/2}$) atoms from

the 467-nm photodissociation of BrCl, including the uncertainties derived from the fitting of linear combinations of images obtained with different configurations of the polarizations of the photolysis and REMPI probe lasers [11, 16]. As explained by Smolin et al. [16], the uncertainties are large because rapid and substantial hyperfine depolarization of the electronic angular momentum polarization of the Cl atoms degrades the signature of the anisotropy parameters in the images.

Given the expressions for the dynamical functions in Table I, equations linking dynamical functions to anisotropy parameters [2, 16, 24], and the 12 values of the anisotropy parameters listed in Table II, a fitting procedure was undertaken to determine the 4 unknown (relative) phases and 5 amplitudes for dissociation via the 5 states that can participate in the dissociation to ground electronic state Br and Cl atoms. The fitting procedure is described in detail below, and is made complicated by the need to obtain amplitudes and phases for coupled dissociation on the $X^1\Sigma^+_{0+}$, $A^3\Pi_1$, $B^3\Pi_{0+}$, $C^1\Pi_1$ and D(1) states portrayed in Fig.1. There are thus numerous parameters to be determined, and the correlations between these parameters must be identified.

The dynamical functions, as expressed in Table I in terms of amplitudes and phases, are linked to the experimentally derived anisotropy parameters (with ranks $K = 0 - 3$) via the following relationships [2, 16, 24]:

$$\begin{aligned}
\beta &= \frac{2[f_0(0,0) - f_0(1,1)]}{f_0(0,0) + 2f_0(1,1)}, \\
\alpha_K &= V_K^{-1}(j)\, \frac{f_K(1,1)}{f_0(0,0) + 2f_0(1,1)}, \\
\gamma_K &= V_K^{-1}(j)\, \frac{2\, Re[f_K(1,0)]}{f_0(0,0) + 2f_0(1,1)}, \\
\gamma'_K &= V_K^{-1}(j)\, \frac{2\, Im[f_K(1,0)]}{f_0(0,0) + 2f_0(1,1)}, \\
\eta_3 &= -\frac{\sqrt{5}}{2} V_3^{-1}(j)\, \frac{Im[f_3(1,-1)]}{f_0(0,0) + 2f_0(1,1)},
\end{aligned} \tag{4}$$

for $K = 1, 3$, with $V_1(j) = 1$ and $V_3(j) = j(j+1)/\sqrt{(j-1)(j+2)(2j-1)(2j+3)}$.

In the case of $K = 2$, the relationships are:

$$\begin{aligned} s_2 &= V_2(j)^{-1}\frac{f_2(0,0)+2f_2(1,1)}{f_0(0,0)+2f_0(1,1)}, \\ \alpha_2 &= V_2(j)^{-1}\frac{f_2(1,1)-f_2(0,0)}{f_0(0,0)+2f_0(1,1)}, \\ \gamma_2 &= 2\sqrt{3}V_2(j)^{-1}\frac{\mathrm{Re}[f_2(1,0)]}{f_0(0,0)+2f_0(1,1)}, \\ \gamma_2' &= 2\sqrt{3}V_2(j)^{-1}\frac{\mathrm{Im}[f_2(1,0)]}{f_0(0,0)+2f_0(1,1)}, \\ \eta_2 &= \sqrt{6}V_2(j)^{-1}\frac{f_2(1,-1)}{f_0(0,0)+2f_0(1,1)}, \end{aligned} \tag{5}$$

with $V_2(j) = 5\{j(j+1)/[(2j+3)(2j-1)]\}^{1/2}$.

The first step was to identify correlations between the anisotropy parameters, and thus reduce the number of equations. In the general case, there are 13 real anisotropy parameters of ranks $K = 0-3$ expressed via Eq. (4,5) which can be represented in terms of 13 real equations connecting them to the dynamical functions of Table I. These functions contain 4 unknown (relative) phases and 5 amplitudes that are to be determined. As is clear from the expressions in Table I and Eqs. (4,5) the anisotropy parameters depend on the ratios of amplitudes, and are independent of their absolute values (which are established by a normalization condition). There are thus 4 unknown (relative) phases and 4 (relative) amplitudes. Using the expressions for the anisotropy parameters in explicit form, the number of non-linear equations can be reduced. In particular, four different correlations between the anisotropy parameters can be expressed by one first-order function, and three second-order functions, which reduces the set of equations to 9 non-linear relationships. The first order function is:

$$\alpha_3 = \frac{1}{V_3(j)\sqrt{35}}\left[\frac{(2-\beta)}{3} - 3\sqrt{15}\left(\alpha_1 - \frac{(2-\beta)}{6\sqrt{15}}\right) + \frac{V_2(j)5\sqrt{5}}{3}(s_2+\alpha_2)\right]. \tag{6}$$

Equation (6) demonstrates the correlation between the anisotropy parameters β, α_1, s_2, α_2, and α_3 in the specific case of the photodissociation of BrCl. Note that eq. (6) is an analytical one, however it fits well the experimentally derived values of the anisotropy parameters β, α_1, s_2, α_2, and α_3 shown in Tab. II within the experimental error bars. Due to the relationship (6), one of the 5 anisotropy parameters can be excluded from the set which will be used in the fit to obtain amplitudes and phases; we choose to exclude the

experimental value of the α_1 anisotropy parameter because of its value close to zero and large relative error.

The second-order functions are not shown here explicitly for reasons of space, but Eq. (7) provides a list of the arguments of each of these functions to illustrate the relevant correlations:

$$\begin{aligned} {}^1S(\beta, \alpha_1, \gamma_1, \gamma_1', s_2, \alpha_2, \alpha_3, \gamma_3, \gamma_3') &= 0, \\ {}^2S(\beta, \alpha_1, s_2, \alpha_2, \eta_2, \eta_3) &= 0, \\ {}^3S(\beta, \alpha_1, \gamma_1, \gamma_1', s_2, \alpha_2, \gamma_2, \gamma_2', \gamma_3, \gamma_3') &= 0, \end{aligned} \tag{7}$$

The function ${}^3S$ in Eq. (7) contains the experimentally undetermined anisotropy parameter γ_2', providing a means to calculate its value directly from the other anisotropy parameters. We therefore have only 8 unknowns, with 9 non-linear equations. This set of non-linear equations is in general incompatible with arbitrary values of the anisotropy parameters, however, so this approach to determination of the amplitudes and phases from experimental anisotropy parameter values is prevented. There remains, however, the possibility to search for solutions to the set of equations within the error bars for the anisotropy parameters, resulting in an optimization problem. With this strategy, we consider the γ_1', and γ_3 anisotropy parameters as additional unknowns; these two parameters are identified in this way because their experimentally determined magnitudes are close to zero, and they carry large relative errors. Fortunately, narrow bounds can be established for most of the unknowns by analytical evaluations from the ranges encompassed by the experimental error bars for the anisotropy parameters. Thus we can consider the bounds defined by the error bars as the feasible region of solution of the optimization problem, and can add a regularizing objective function. The resultant optimization problem was solved using well-established procedures as described, for example, in [26, 27].

The values of the amplitudes and phases derived from the analysis are listed in Table III, and the outcomes were verified by using them to recalculate the experimental anisotropy parameters. As shown in the final column of Table II, the values of the anisotropy parameters obtained from the fitted **T**-matrix element amplitudes and phases lie within the uncertainty ranges of the experimental measurements, with a few exceptions. In some cases, such as the values of α_1 and γ_1', the discrepancies between the experimental values and the fit outcomes

are not significant because the values taken by these parameters are so close to zero. The fit outcomes successfully capture the small magnitudes of these two anisotropy parameters. The γ_3 and γ_3' parameters depend upon the $f_3(1,0)$ dynamical function and thus are very sensitive to small changes in any of the amplitudes and phases that are determined in the optimization. Small discrepancies between the calculated and experimental values of certain anisotropy parameters may also be a consequence of over-evaluation of the experimental precision.

The data in Table III contain important new information about the photodissociation dynamics of BrCl which has not been considered previously. The deconvolution of the absorption spectrum of BrCl at wavelengths in the visible and near-UV regions of the spectrum demonstrated that the initial excited state amplitude is on the $A^3\Pi_1$, $B^3\Pi_{0+}$ and $C^1\Pi_1$ states [20], but the results presented in Table III demonstrate that there is substantial (and quantifiable) accumulation of dissociative flux on the $X^1\Sigma_{0+}^+$ and D(1) states because of non-adiabatic dynamics. The flux on the $B^3\Pi_{0+}$ state, which is strongly excited at 467 nm, is significantly depleted by transfer to the $X^1\Sigma_{0+}^+$ state. At 467 nm, the deconvolution of the absorption spectrum by Beckert et al. [20] suggests that excitation to the $A^3\Pi_1$ state dominates the other possible perpendicular transition to the $C\,^1\Pi_1$ state, and thus that $C\,^1\Pi_1$ and D(1) states are populated by depletion of flux on the $A^3\Pi_1$ state potential. At what points on the adiabatic potential energy curves these non-adiabatic transitions occur is not a question that is answered by our measurements and analysis, but the non-adiabatic dynamics are likely to occur at large internuclear separations where the spacings between the potentials become small and the molecule undergoes a recoupling of its electronic angular momentum to evolve into wavefunctions corresponding to the separated atoms [28].

The scattering phase differences in Table III, if interpreted in the quasiclassical approximation [29] will, in general, contain two contributions. One of these contributions is related to the coherence between states of different symmetry ($\Omega = 0$ and $\Omega = \pm 1$) [6] (note that the coherence between states with the same Ω does not give a contribution to the signal [4]). The associated phase shift is mostly due to the nuclear motion on PE curves of different shapes in the adiabatic region and can be associated with the elastic scattering phase shift. The other contribution is a dynamical phase shift between states of the same symmetry, and is due to electronic and nuclear motion in the vicinity of the non-adiabatic interaction regions that occur in the locality of quasi (i.e., partially avoided) crossings, and at large

internuclear separations. As shown in Table III the phase shifts are large in magnitude. Both contributions to the phases are important for BrCl at wavelengths in the visible and near-UV regions of the spectrum. The contributions can in principle be separated by consideration of the data in Tables I and III. In particular, as is seen from the expressions for $f_1(1,1)$ and $f_1(1,0)$ in Table III, the phase difference $\phi_A - \phi_C$ is of the "dynamical" type, while the phase differences $\phi_B - \phi_A$, $\phi_X - \phi_C$, $\phi_B - \phi_D$, and $\phi_X - \phi_D$ are of the "coherent" type.

III. CONCLUSIONS

Values of all except one of the rank $K = 0, 1, 2$ and 3 $\mathrm{Cl}(^2P^0_{3/2})$ angular momentum anisotropy parameters for the 467-nm, one-photon photodissociation of BrCl, previously determined by velocity map imaging experiments [11, 16], have been inverted to quantify the dynamical functions, amplitudes and relative phases of the nuclear wavefunctions on all five of the potential energy curves involved in the dissociation. The derived amplitudes and phases constitute the components of the photofragmentation **T**-matrix, and the current study is thus a realization of a "complete" photodissociation experiment at one excitation wavelength. Following photoexcitation on both parallel and perpendicular transitions to states with $\Omega = 0^+$ and 1, we show there to be significant amplitude of dissociative nuclear wavefunctions on all of the $X^1\Sigma^+_{0+}$, $A^3\Pi_1$, $B^3\Pi_{0+}$, $C^1\Pi_1$ and D(1) states, which adiabatically correlate asymptotically to $\mathrm{Cl}(^2P^0_{3/2})$ + $\mathrm{Br}(^2P^0_{3/2})$ products. The excitation at this wavelength was previously determined to be primarily to the $A^3\Pi_1$ and $B^3\Pi_{0+}$ states, and subsequent non-adiabatic dynamics, most likely occurring at large internuclear separations, populates the other three states. The phases of the nuclear wavefunctions on the $A^3\Pi_1$, $B^3\Pi_{0+}$, $C^1\Pi_1$ and D(1) states, specified relative to that on the $X^1\Sigma^+_{0+}$ state, are all markedly different, in part because of phase shifts induced in the region of internuclear separations where non-adiabatic dynamics occurs.

Acknowledgments

A.G.S. acknowledges support from the INTAS grant N 03-55-1277. AJOE thanks the EPSRC for the award of the LASER Portfolio Partnership grant, and the Leverhulme Trust

for a Senior Research Fellowship. We thank O.P.J. Vieuxmaire, Prof M.N.R. Ashfold, and Drs E.R. Wouters and M. Beckert for their respective contributions to the work described herein.

[1] L. D. A. Siebbeles, M. Glass-Maujean, O. S. Vasyutinskii, J. A. Beswick and O. Roncero, J. Chem. Phys. **100**, 3610 (1994).

[2] G. G. Balint-Kurti, A. J. Orr-Ewing, J. A. Beswick, A. Brown and O. S. Vasyutinskii, J. Chem. Phys., **116**, 10760 (2002).

[3] G. G. Balint-Kurti, A. Brown and O. S. Vasyutinskii, J. Phys. Chem.A, **108**, 7790 (2004).

[4] E. R. Wouters, M. Ahmed, D. S. Peterka, A. S. Bracker, A. G. Suits and O. S. Vasyutinskii, "Imaging the Atomic Orientation and Alignment in Photodissociation" in *Imaging in Chemical Dynamics*, A. G. Suits and R. E. Continetti, eds., (American Chemical Society, Washington DC, 2000), p.238.

[5] G. G. Balint-Kurti and M. Shapiro, Chem. Phys., **61**, 137 (1981).

[6] T. P. Rakitzis, S. A. Kandel, A. J. Alexander, Z. H. Kim and R. N. Zare, Science, **281**, 1346 (1998).

[7] A. T. J. B. Eppink, D. H. Parker, M. H. M. Janssen, B. Buijsse, B. and W. J. van der Zande, J. Chem. Phys., **108**, 1305 (1998).

[8] A. S. Bracker, E. R. Wouters, A. G. Suits and O. S. Vasyutinskii, J. Chem. Phys., **110**, 6749 (1999).

[9] T. P. Rakitzis and R. N. Zare, J. Chem. Phys., **110**, 3341 (1999).

[10] A. J. Alexander, Z. H. Kim, S. A. Kandel, R. N. Zare, T. P. Rakitzis, Y. Asano and S. Yabushita, J. Chem. Phys., **113**, 9022 (2000).

[11] E. R. Wouters, M. Beckert, L. J. Russell, K. N. Rosser, A. J. Orr-Ewing, M. N. R. Ashfold and O. S. Vasyutinskii, J. Chem. Phys., **117**, 2087 (2002).

[12] T. P. Rakitzis, P. C. Samartzis, R. L. Toomes, L. Tsigaridas, M. Coriou, D. Chestakov, A. T. J. B. Eppink, D. H. Parker, and T. N. Kitsopoulos, Chem. Phys. Lett. **364**, 115 (2002).

[13] T. P. Rakitzis, P. C. Samartzis, R. L. Toomes, and T. N. Kitsopoulos, J. Chem. Phys. **121**, 7222 (2004).

[14] M. J. Bass, M. Brouard, A. P. Clark, C. Vallance, and B. Martinez-Haya, Phys. Chem. Chem. Phys. **5**, 856 (2003).

[15] K. O. Korovin, B. V. Picheyev, O. S. Vasyutinskii, H. Valipour, and D. Zimmermann, J. Chem. Phys., **112**, 2059 (2000).

[16] A. G. Smolin, O. S. Vasyutinskii, O. P. J. Vieuxmaire, M. N. R. Ashfold, G. G. Balint-Kurti and A. J. Orr-Ewing, J. Chem. Phys., **124**, 094305 (2006).

[17] A. J. Alexander and T. P. Rakitzis, Mol. Phys., **103**, 1665 (2005).

[18] K. O. Korovin, V. V. Veselov, E. M. Mikheev, O. S. Vasyutinskii, and D. Zimmermann, Optics and Spectroscopy, **99**, 880 (2005).

[19] M. J. Cooper, P. J. Jackson, L. J. Rogers, A. J. Orr-Ewing, M. N. R. Ashfold and B. J. Whitaker, J. Chem. Phys., **109**, 4367 (1998).

[20] M. Beckert, E. R. Wouters, M. N. R. Ashfold and E. Wrede, J. Chem. Phys., **119**, 9576 (2003).

[21] D. A Varshalovich, A. N. Moskalev and V. K. Khersonskii, *Quantum Theory of Angular Momentum*; World Scientific: Singapore, 1988.

[22] R. N. Zare, *Angular Momentum*; World Scientific: New York, 1988.

[23] W. Happer, Rev. Mod. Phys., **44**, 169 (1972).

[24] B. V. Picheyev, A. G. Smolin, and O. S. Vasyutinskii, J. Phys. Chem., **101**, 7614 (1997).

[25] G. G. Balint-Kurti, A. Brown, and O. S. Vasyutinskii, Physica Scripta, **73**, C76 (2006).

[26] M. A. Diniz-Ehrhardt, J. M. Martínez, "Successive Projection Methods for the Solution of Overdetermined Nonlinear Systems" in *Nonlinear Optimization and Applications*, G. Di Pillo and F. Giannessi ed. (Plenum Publishing Corporation, 1996), p.75.

[27] J. E. Dennis Jr., "Nonlinear least-squares" in *State of the Art in Numerical Analysis*, D. Jacobs ed. (Academic Press, London, 1977) pp. 269-312.

[28] P. M. Regan, D. Ascenzi, A. Brown, G. G. Balint-Kurti and A. J. Orr-Ewing, J. Chem. Phys., **112**, 10259 (2000).

[29] E. E. Nikitin and S. Ya. Umanskii, *Theory of Slow Atomic Collisions;* Springer: Berlin, 1984.

TABLE I: Expressions for the $K = 1$ to 3 dynamical functions for Cl($^2P^0_{3/2}$) atoms from the photodissociation of BrCl.

Dynamical function	*Expression*
$f_0(1,1)$	$\frac{1}{2}\left(r_A^2 + r_C^2 + r_D^2\right)$
$f_0(0,0)$	$\frac{1}{2}\left(r_B^2 + r_X^2\right)$
$f_1(1,1)$	$\frac{1}{2\sqrt{15}}\left(r_A^2 + r_C^2 + r_D^2 + 4r_A r_C \cos(\phi_A - \phi_C)\right)$
$f_1(1,0)$	$\frac{1}{2\sqrt{5}}\left(r_A r_B e^{i(\phi_B-\phi_A)} - r_C r_X e^{i(\phi_X-\phi_C)} - \frac{\sqrt{6}}{3} r_D r_B e^{i(\phi_B-\phi_D)} + \frac{\sqrt{6}}{3} r_D r_X e^{i(\phi_X-\phi_D)}\right)$
$f_1(1,-1)$	0
$f_2(1,1)$	$-\frac{1}{2\sqrt{5}}\left(r_D^2 - 2r_A r_C \cos(\phi_A - \phi_C)\right)$
$f_2(0,0)$	$\frac{1}{\sqrt{5}}\, r_B r_X \cos(\phi_B - \phi_X)$
$f_2(1,0)$	$-\frac{1}{2\sqrt{5}}\left(r_A r_X e^{i(\phi_X-\phi_A)} - r_C r_B e^{i(\phi_B-\phi_C)}\right)$
$f_2(1,-1)$	$-\frac{1}{\sqrt{5}}\left(r_A r_D \cos(\phi_A - \phi_D) + r_C r_D \cos(\phi_C - \phi_D)\right)$
$f_3(1,1)$	$\frac{1}{\sqrt{35}}\left(r_A^2 + r_C^2 - \frac{3}{2} r_D^2 - r_A r_C \cos(\phi_A - \phi_C)\right)$
$f_3(1,0)$	$\frac{1}{\sqrt{70}}\left(r_A r_B e^{i(\phi_B-\phi_A)} - r_C r_X e^{i(\phi_X-\phi_C)} + \sqrt{\frac{3}{2}} r_D r_B e^{i(\phi_B-\phi_D)} - \sqrt{\frac{3}{2}} r_D r_X e^{i(\phi_X-\phi_D)}\right)$
$f_3(1,-1)$	$\frac{i}{\sqrt{7}}\left(r_C r_D \sin(\phi_C - \phi_D) + r_A r_D \sin(\phi_A - \phi_D)\right)$

TABLE II: Rank $K = 0, 1, 2$ and 3 anisotropy parameters determined from fits to experimental velocity map images for Cl($^2P^0_{3/2}$) atoms from the 467 nm photodissociation of BrCl. The numbers in parentheses are 1σ uncertainties in the last significant digit(s). The value of γ'_2 is evaluated from the optimization procedure, but was not measured experimentally.

Parameter	*Experimental value*	*Range*	*Calculated from fit*
β	0.06(2)	-1 to 2	0.06
α_1	0.009(5)	-0.250 to 0.250	0.028
γ_1	$-0.14(5)$	-0.524 to 0.524	-0.16
γ'_1	0.015(6)	-0.524 to 0.524	0.030
α_2	$-0.068(6)$	-0.108 to 0.108	-0.062
s_2	$-0.028(4)$	-0.16 to 0.16	-0.032
γ_2	0.114(4)	-0.162 to 0.162	0.135
γ'_2	—	-0.162 to 0.162	-0.080
η_2	$-0.041(9)$	-0.155 to 0.155	-0.041
α_3	0.11(5)	-0.201 to 0.201	0.062
γ_3	0.12(6)	-0.353 to 0.353	0.010
γ'_3	0.093(42)	-0.353 to 0.353	0.118
η_3	$-0.072(31)$	-0.236 to 0.236	-0.097

TABLE III: Amplitudes and phases of the nuclear wavefunctions on the $X^1\Sigma^+_{0+}$, $A^3\Pi_1$, $B^3\Pi_{0+}$, $C^1\Pi_1$ and D(1) states for 467 nm photodissociation of BrCl to form Cl($^2P^0_{3/2}$) atoms. The last line represents the experimental value of the amplitude corresponding to population of the Br+Cl* channel [20]. The amplitude values are normalized to unity.

State (n)	r_n	$\phi_n - \phi_X$ / *radians*
$X^1\Sigma^+_{0+}$	0.395	0
$A^3\Pi_1$	0.325	−2.64
$B^3\Pi_{0+}$	0.120	−0.224
$C^1\Pi_1$	0.082	0.789
D(1)	0.201	2.49
Br + Cl*	0.820	–

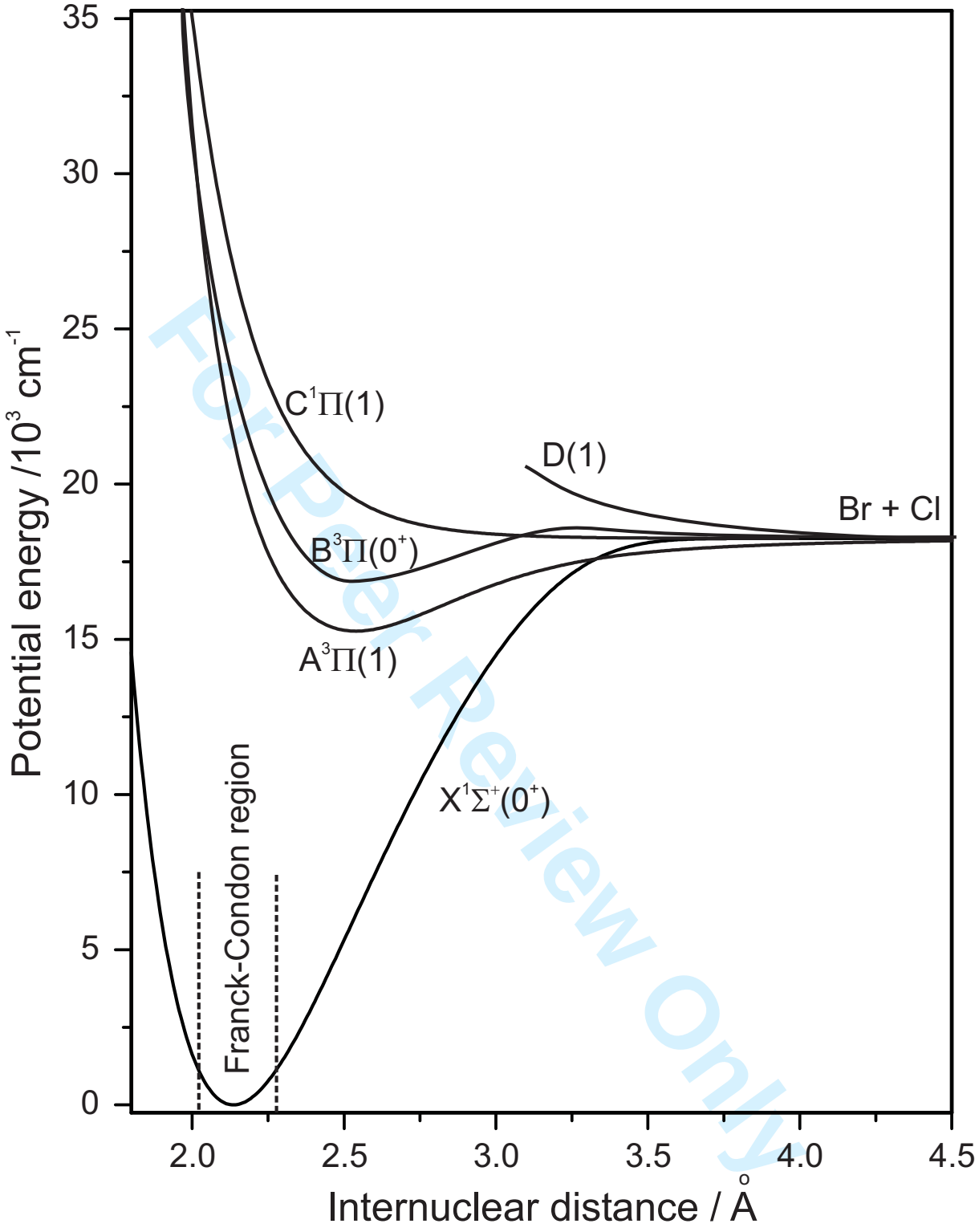

FIG. 1: Potential energy curves for the five electronic states involved in the production of Cl($^2P^0_{3/2}$) atoms from the 467-nm photodissociation dynamics of BrCl. The curves for the X, A, B and C states are based on the accurate empirical curves of Beckert et al. [20]; the D-state curve is schematic.